




Title	Role of NPPB for recovery post ventricular assist device in paediatric dilated cardiomyopathy : Single-cell multiomics
Author(s)	Kugo, Yosuke; Kawamura, Takuji; Harada, Akima et al.
Citation	ESC Heart Failure. 2025
Version Type	VoR
URL	https://hdl.handle.net/11094/102973
rights	This article is licensed under a Creative Commons Attribution-NonCommercial-NoDerivatives 4.0 International License.
Note	

The University of Osaka Institutional Knowledge Archive : OUKA

<https://ir.library.osaka-u.ac.jp/>

The University of Osaka

Role of *NPPB* for recovery post ventricular assist device in paediatric dilated cardiomyopathy: Single-cell multiomics

Yosuke Kugo¹, Takuji Kawamura^{1*}, Akima Harada¹, Yuji Tominaga², Kenji Miki³, Hidekazu Ishida⁴, Takayoshi Ueno⁵ and Shigeru Miyagawa^{1*} 

¹Department of Cardiovascular Surgery, Graduate School of Medicine Faculty of Medicine, The University of Osaka, Suita, Japan; ²Department of Pediatric Cardiovascular Surgery, National Cerebral and Cardiovascular Center, Suita, Japan; ³Premium Research Institute for Human Metaverse Medicine, The University of Osaka, Suita, Japan; ⁴Department of Pediatrics, Graduate School of Medicine Faculty of Medicine, The University of Osaka, Suita, Japan; and ⁵Division of Health Sciences, Graduate School of Medicine, The University of Osaka, Suita, Japan

Abstract

Aims Paediatric heart transplantation requires lifelong immunosuppression, highlighting the need for recovery-oriented strategies. A subset of children with dilated cardiomyopathy (DCM) recovers left ventricular (LV) function after LV assist device (LVAD) implantation, allowing for device explantation. We aimed to identify factors associated with LV functional recovery using single-nucleus multiomics analysis of LV tissue collected at LVAD implantation.

Methods We included children with idiopathic DCM who underwent LVAD implantation between 2013 and 2023. Patients who achieved device explantation and medical stabilization were classified as the recovery group while those who required transplantation or died were classified as the non-recovery group. Single-nucleus RNA and ATAC sequencing were performed in six representative cases. Differential gene expression, chromatin accessibility and gene ontology (GO) enrichment analyses were conducted. Candidate markers were validated histologically and serologically in the full cohort.

Results Twenty-five cases were included (non-recovery, $n = 15$; recovery, $n = 10$). Age at LVAD implantation [median (range)] was 0.9 (0.1–4.6) versus 0.8 (0.3–5.6) years ($P = 0.8$), sex 27% versus 30% male ($P > 0.9$) and body weight 5.9 (3.8–14.0) versus 7.5 (5.0–26.0) kg ($P = 0.049$). LV ejection fraction at implantation was similar (24 (10–44) % vs. 15 (10–25) %, $P = 0.2$). RNA sequencing showed elevated *NPPB*, *MYL7* and *PCDH9* in recovery-group cardiomyocytes, with *NPPB* highest expression [baseMean = 16 305; log₂Fold Change (FC) = 2.698; $P < 0.001$] and an accessible chromatin peak at its locus (log₂FC = 1.17; $P < 0.01$). GO analysis indicated enrichment in apoptosis-related pathways (coefficient = 1.77, $P = 0.023$). Serum brain natriuretic peptide (BNP), the protein product of *NPPB*, was significantly higher in the recovery group at implantation [732 (372–4179) vs. 3048 (642–6032) pg/mL, $P = 0.04$] as was the proportion of non-apoptotic cardiomyocytes [0.21 (0.02–0.37) vs. 0.37 (0.19–0.48), $P = 0.03$].

Conclusions Elevated *NPPB* expression and BNP levels at LVAD implantation are associated with LV recovery in paediatric DCM. These findings support an anti-apoptotic role of BNP in successful bridge-to-recovery outcomes.

Paediatric DCM exhibits significant heterogeneity in both genetic background and phenotype,^{7–9} and the effects of LV unloading on myocardial tissue involve various molecular pathways.^{10,11} Given the expected complexity of the preoperative factors influencing bridge-to-recovery outcomes, a comprehensive approach is essential to elucidate the cellular and molecular mechanisms involved.

Single-cell RNA sequencing enables cellular-level gene expression profiling, and the assay for transposase-accessible chromatin (ATAC) sequencing reveals the epigenetic landscape by analysing open chromatin regions within individual cells or cell types, which could lead to a better understanding of molecular mechanisms.^{12,13} In this study, we aimed to explore intracellular molecular characteristics to achieve the bridge-to-recovery approach using a single-nucleus multiomics analysis of myocardial tissue samples extracted during LVAD implantation.

Methods

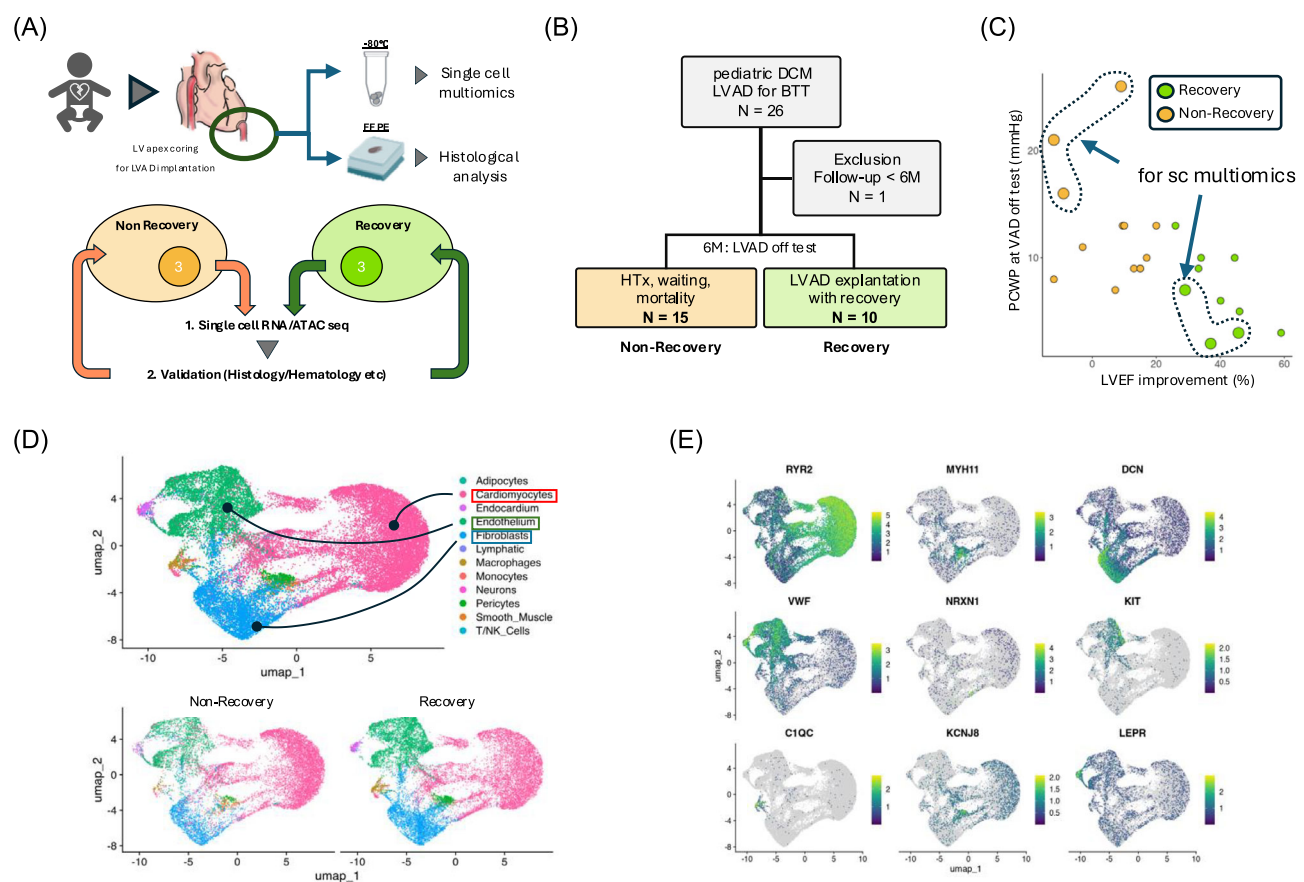
Ethical statement

This study complied with the Declaration of Helsinki and was approved by the Institutional Ethics Committee of Osaka University Hospital [approval date: 22 August 2023; approval number: 23135(T3)-3]. Written informed consent was obtained from all participants and/or legal guardians.

Overview

Paediatric patients with idiopathic DCM undergoing bridge-to-transplant LVAD (BTT-LVAD) implantation at our institution were divided into recovery and non-recovery groups based on sustained LV function after LVAD implantation.

Figure 1 Overview of the study and single nuclei analysis. (A) Top: description of myocardial tissue collection and preservation. Bottom: three cases are extracted from each outcome group, single nuclei multiomics are performed, and validation is attempted on all cases based on the omics results. (B) Patients' selection flow. (C) A scatter plot showing LVEF improvement and PCWP at 6 months after LVAD implantation. Colours indicate the outcome group. The large points indicate typical clinical presentations, which are selected for single nucleus multiomics. (D) UMAP plots and cell type labelling for all cells after integration of a total of six samples. Cardiomyocytes, fibroblasts and endothelium make up a large portion, with no significant unbalanced distribution among each outcome group. (E) Feature plots of representative marker genes in each cell type. DCM, dilated cardiomyopathy; HTx, heart transplantation; LV, left ventricle; LVAD, left ventricular assist device; FFPE, formalin fixed paraffin embedded; RNA/ATAC seq, ribonucleic acid/the assay for transposase-accessible chromatin with sequencing.



Three representative cases from each group underwent single-nucleus RNA–ATAC sequencing of LV tissue obtained at implantation to identify candidate genes. These were then evaluated in the whole cohort using histological and serological analyses (Figure 1A).

Patients

Inclusion criteria were as follows: (1) age ≤ 15 years, (2) idiopathic DCM diagnosed according to the 2023 European Society of Cardiology guidelines⁹ and (3) Berlin Heart EXCOR implantation as BTT between January 2013 and December 2023. Secondary cardiomyopathies and fulminant myocarditis were excluded. Patients with <6 months follow-up after LVAD implantation were also excluded.

All received maximal medical therapy including beta-blockers, angiotensin-converting enzyme inhibitors (ACEIs) and diuretics preoperatively; those with persistent severe heart failure despite inotropes underwent LVAD implantation. Postoperatively, all received adequate support (cardiac index ≥ 2.5) and guideline-directed medical therapy for heart failure.

LVAD implantation, myocardial tissue collection and preservation

EXCOR implantation was performed via median sternotomy under cardiopulmonary bypass. LV apical tissue was collected at coring: one portion was frozen at -80°C , another fixed in 10% formalin and embedded in paraffin.

LVAD off test and definition of outcomes

At 6 months post-LVAD implantation, patients who did not demonstrate LV functional recovery on echocardiography and exhibited strong dependence on LVAD support were excluded from the off-test protocol. Others underwent stepwise support reduction during catheterization. Those meeting published recovery criteria¹⁴ (or approximating them) were considered for explantation, with the final decision based on overall clinical assessment.

Recovery cases were defined as stable LV function after explantation without inotropes and delisting for transplant. Non-recovery cases included failure to meet these criteria or deterioration after explantation requiring re-LVAD implantation, heart transplantation or experiencing mortality.

Single-nucleus RNA/ATAC sequencing

From six representative patients (three per group), frozen LV tissue underwent nuclei isolation,^{15,16} library preparation

(10× Genomics Chromium Multiome), sequencing (NovaSeq 6000), and bioinformatic analysis (Seurat, Signac, DESeq2, iDEA, CellChat). Quality control thresholds, reference datasets,¹⁷ and analytical parameters are provided in the Data S2. Figure 1C shows a scatter plot of the LVEF improvement rates (defined as the LVEF at the time of the VAD-off test minus the LVEF immediately before implantation, %) versus PCWP during the VAD-off test. The large data points in the figure indicate the cases selected for single-cell analysis.

Validation of candidate genes across all cases

Candidate genes identified by multiomic analysis were validated histologically and serologically in the full patient cohort. LV tissue was analysed by haematoxylin and eosin, Masson's trichrome and TUNEL staining, and serum biomarkers were quantified from perioperative samples. Image analysis was performed using standardized region-of-interest and thresholding protocols.^{5,6} Full staining protocols and image analysis parameters are available in the Data S2.

Statistics for non-omics data

Continuous variables are reported as medians (range), categorical as n (%). Group comparisons used Wilcoxon rank-sum or Fisher's exact test; correlations used Pearson's r . LV dimensions were indexed to body surface area using Kampmann's equation.¹⁸

Results

Patients and clinical outcomes

As Figure 1B shows, a total of 26 paediatric patients with DCM underwent EXCOR implantation for BTT-LVAD. One patient received a heart transplant 1 month after implantation and was excluded from the analysis, leaving 25 patients for evaluation. Among them, 15 cases were classified as non-recovery cases and 10 as recovery cases. Table 1 shows the preoperative patient characteristics. The body weight at implantation was lower in the non-recovery cases than in the recovery cases [non-recovery: 5.9 (3.8–14.0) kg vs. recovery: 7.5 (5.0–26.0) kg, $P = 0.049$], while the age at LVAD implantation was similar in both cases [non-recovery: 0.9 (0.1–4.6) years vs. recovery: 0.8 (0.3–5.6) years, $P = 0.8$]. The time from diagnosis to LVAD implantation was longer in non-recovery cases than in recovery cases [non-recovery: 6.0 (1.0–37.0) months vs. recovery: 2.0 (0.0–15) months, $P = 0.04$], although the age at diagnosis was older in recovery cases. There were no significant differences in the indexed

Table 1 Patients characteristics.

Characteristic	Non-recovery, <i>N</i> = 15 ^a	Recovery, <i>N</i> = 10 ^a	<i>P</i> value ^b
Sex (male)	4 (27%)	3 (30%)	>0.9
Age (years)	0.9 [0.1–4.6]	0.8 [0.3–5.6]	0.8
Body weight (kg)	5.9 [3.8–14.0]	7.5 [5.0–26.0]	0.049
Pre-MCS	4 (27%)	3 (30%)	>0.9
Age at diagnosis (months)	3.0 [0.0–48.0]	10.0 [1.0–60.0]	0.016
Pre-LVEF (%)	24.0 [10.0–44.0]	15.0 [10.0–25.0]	0.2
Pre-LVDD (%)	173.5 [135–237]	189.5 [129–229]	0.6
Pre-PCWP (mmHg)	23.0 [14.0–33.0]	16.0 [14.0–23.0]	0.15

Note: All variables with prefixes pre- indicate values from catheterization prior to left ventricular assist device implantation.

Abbreviations: LVDD, left ventricular diameter of diastolic phase; LVEDP, left ventricular end diastolic pressure; LVEF, left ventricular ejection fraction; MCS, mechanical circulatory support; PAP, pulmonary arterial pressure.

^a*n* (%); median [min–max].

^bFisher's exact test; Wilcoxon rank sum test; Wilcoxon rank sum exact test.

Table 2 Perioperative pharmacological characteristics.

Medication	Patients, <i>n</i> (%)			Mean daily dose		
	Non-recovery (<i>N</i> = 15)	Recovery (<i>N</i> = 10)	<i>P</i> value	Non-recovery (<i>N</i> = 15)	Recovery (<i>N</i> = 10)	<i>P</i> value
Preoperative						
Carvedilol (mg/kg/day)	12 (86%)	8 (80%)	>0.9	0.10 [0.01–0.46]	0.05 [0.04–0.30]	0.5
Enalapril (mg/kg/day)	14 (93%)	7 (70%)	0.3	0.16 [0.10–0.53]	0.10 [0.03–0.34]	0.10
Furosemide (mg/kg/day)	15 (100%)	10 (100%)	NA	3.10 [0.40–9.60]	5.25 [1.40–9.00]	0.3
Digoxin (μg/kg/day)	3 (20%)	1 (10%)	0.6	5.0 [2.0–10]	10.0	>0.9
Postoperative						
Carvedilol (mg/kg/day)	14 (93%)	10 (100%)	>0.9	0.20 [0.05–0.50]	0.21 [0.10–0.40]	0.6
Enalapril (mg/kg/day)	15 (100%)	10 (100%)	NA	0.20 [0.10–0.42]	0.23 [0.10–0.40]	>0.9
Furosemide (mg/kg/day)	13 (87%)	6 (60%)	0.2	2.00 [0.90–3.75]	1.20 [0.50–5.10]	0.8
Digoxin (μg/kg/day)	0 (0%)	0 (0%)	NA	—	—	—

Note: Values are presented as the number of patients (*n*) with the percentage in parentheses for the proportion of patients, and as median [range] for drug dosages, respectively. Furosemide doses represent the total of both intravenous and oral administration. Digoxin doses are expressed in μg/kg/day, whereas all other drugs are expressed in mg/kg/day. *P* values were calculated using the Wilcoxon rank-sum test or Fisher's exact test, as appropriate.

Abbreviation: NA, not applicable.

LVDD [non-recovery: 173.5 (135–237) vs. recovery: 189.5 (129–229), *P* = 0.6] or LVEF based on echocardiographic long-axis views [non-recovery: 24.0 (10–44) % vs. recovery: 15 (10–25) %, *P* = 0.2]. The PCWP on preoperative catheterization tended to be higher in non-recovery cases, but this difference was not significant [non-recovery: 23.0 (14–33) mmHg vs. recovery: 16.0 (14–23) mmHg, *P* = 0.2]. Postoperative LVAD support levels did not differ significantly [non-recovery: 2.86 (1.74–3.76) L/min/m² vs. recovery: 2.55 (1.14–3.43) L/min/m², *P* = 0.2]. Representative drugs (carvedilol, enalapril, furosemide and digoxin) are summarized in Table 2. Preoperative carvedilol usage was similar (non-recovery: 86% vs. recovery: 80%, *P* > 0.9), as was enalapril usage (non-recovery: 93% vs. recovery: 70%, *P* = 0.3). Postoperatively, carvedilol was used at comparable rates (non-recovery: 93% vs. recovery: 100%, *P* > 0.9), and enalapril was used in all patients in both groups. Furosemide was used preoperatively in all patients; postoperatively, usage tended to be lower in the recovery group (non-recovery: 87% vs. recovery: 60%, *P* = 0.2).

During the LVAD-off test in the recovery cases, the PCWP was 6 (3–10) mmHg, the cardiac index (thermodilution) was

4.6 (3.9–6.4) L/min/m², and the indexed pulmonary vascular resistance was 1.4 (0.5–3.4) Wood units (WU)·m². The follow-up period after LVAD explantation was 5.3 (1.4–8.2) years. In all recovery cases, inotropes were successfully discontinued, and the patients were managed with oral medications such as ACEIs and beta-blockers to be withdrawn from the transplant waiting list. Results of the LVAD-off test among recovery cases are shown in Table S1.

Genetic panel testing for cardiomyopathy-related genes for the six cases included in the single-cell analysis showed that one recovery case exhibited a missense mutation in *MYH7*, while one non-recovery case exhibited a variant of uncertain significance, LDB3 c.2017G > A. No mutations were detected in the remaining four cases. The list of genes included in the panel is shown in Data S1.

Single-nucleus RNA/ATAC sequencing

Cell filtering and labelling

The number of nuclei per sample prior to cell filtering was 8897 (3142–14 410), with an average of 7323 (1541–8831)

nuclei retained after filtering. Cell labelling using published single-cell analysis data categorized the nuclei into 15 cell types. The most abundant cell type was cardiomyocytes, followed by fibroblasts and vascular endothelial cells (Figure 1D,E). The remaining cells (immunocompetent cells and neurons) were few in number and not labelled with high quality to withstand further analysis and discussion. A summary of the metrics for each sample, including quality control metrics for the gene expression matrix, features of dimensional reduction, prediction scores for cell labelling and QC metrics for ATAC data, is presented in Table S2 and Figures S1 and S2. In the subsequent analysis, the results are presented for the three cell types with adequate accuracy and cell counts.

Cardiomyocytes

By isolating cardiomyocytes and performing pseudobulk differentially expressed gene (DEG) analysis, increased expression of genes such as *NPPB*, *MYL7* and *PCDH9* was observed in recovery cases, whereas *KCNIP2* and *KCNMB2* were elevated in non-recovery cases (Figure 2A). Similarly, pseudobulk differential accessibility region (DAR) analysis using ATAC sequencing data revealed alterations in chromatin accessibility for several structural genes (Figure 2B). Among these, *NPPB*, which exhibited significantly increased expression in the recovery group, also showed higher enriched chromatin accessibility with the highest baseline expression among the examined genes.

Figure 2 Single-nuclei (sn) RNA/ATAC seq results in cardiomyocytes. (A) A volcano plot of pseudobulk differentially expressed gene analysis from snRNA sequencing. Horizontal axis indicates fold change, vertical axis indicates significance, and point size indicates the baseline expression levels. (B) A volcano plot of pseudobulk differential accessibility region analysis from sn ATAC sequencing. Labelled point indicates genes found significant in differentially expressed gene analysis, where *NPPB* is included. (C,D) Unsupervised clustering in cardiomyocytes. Although 14 subclusters are classified, the set of genes characterizing each cluster does not include the major genes, such as *NPPB*, that showed alterations in the pseudobulk analysis. (E) Violin plots showing *NPPB* gene expression in 14 subclusters. In all subclusters, expression is upregulated in recovery cases. (F) Coverage plot showing Tn5 insertion frequency over *NPPB* and adjacent region. Both *NPPB* and *NPPA* showed significant high frequency in recovery cases, with links to both genes. RNA/ATAC sequencing: ribonucleic acid/the assay for transposase-accessible chromatin with sequencing.

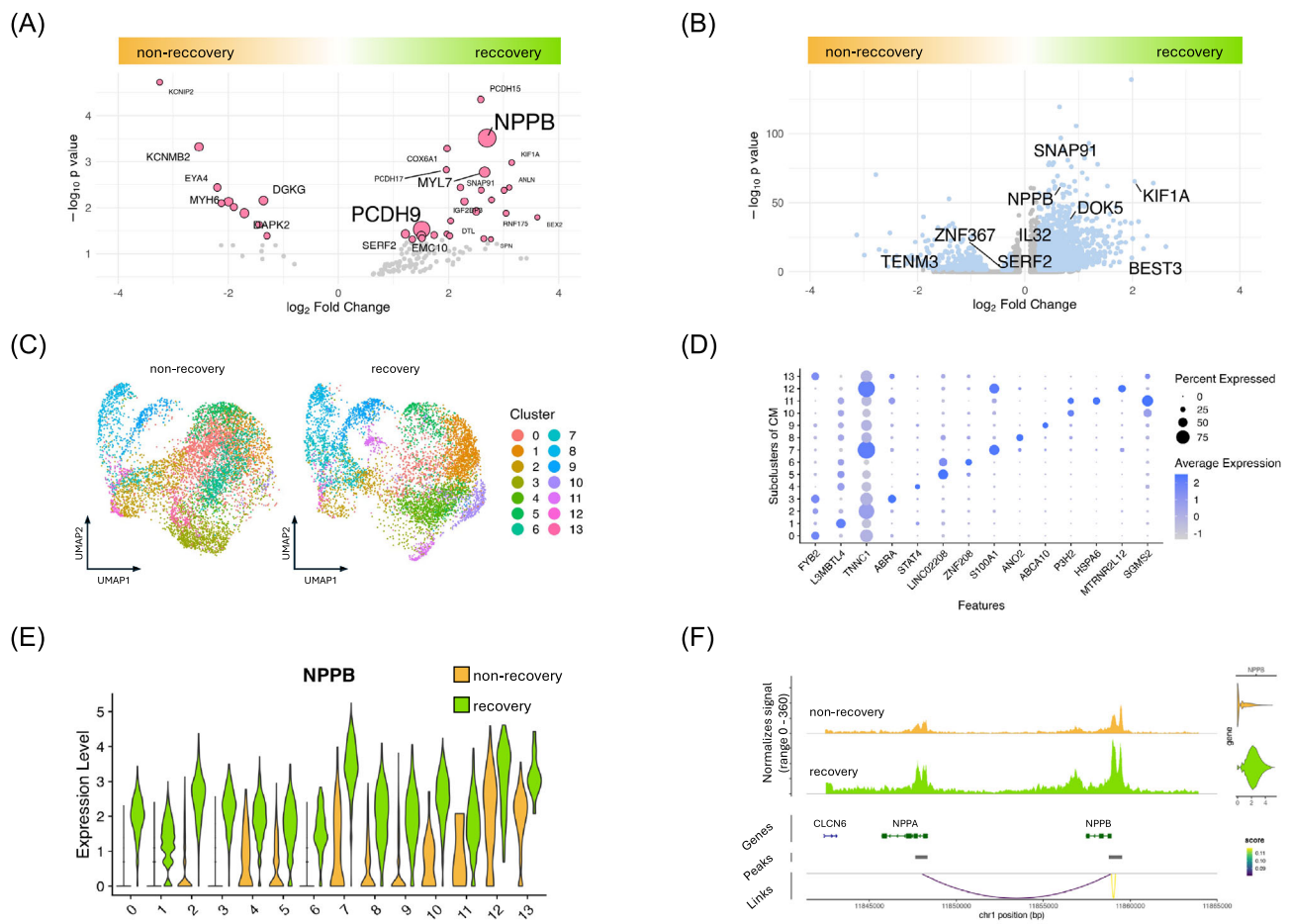
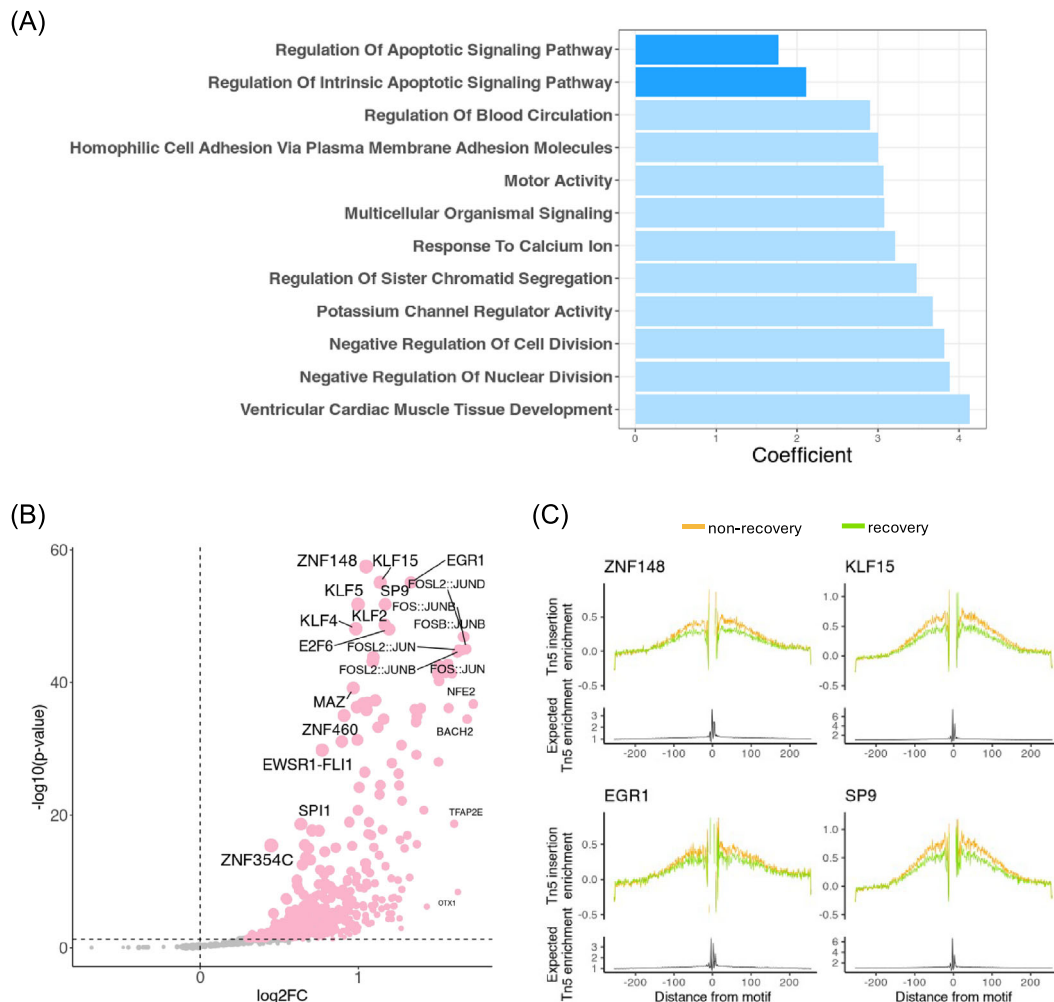


Figure 3 Gene set enrichment and motif analyses in cardiomyocytes. (A) The pathways that showed significant alteration in gene ontology are shown. Alteration is found in pathways related to apoptosis regulation and cell division. (B) A volcano plot of motif analysis using ATAC sequence results. Horizontal axis shows fold change and vertical axis shows significance. (C) Results of footprint analysis of transcription factors that are significant in the Motif analysis. All show increased activity in non-recovery groups. ATAC, assay for transposase-accessible chromatin.



The unsupervised clustering of cardiomyocytes identified 13 subclusters, whereas *NPPB* was not among the top five defining features (ranked by fold change) for any specific subcluster. Instead, it showed consistent expression differences across all subclusters between the recovery and non-recovery groups (Figure 2C–E). The chromatin accessibility of *NPPB* was associated with that of *NPPA*, and both showed elevated peaks (Figure 2F). Gene Ontology pathway analysis using pseudobulk DEG results via integrated gene set enrichment analysis highlighted changes in pathways associated with ventricular cardiac muscle tissue development, motor activity (sarcomere-related pathways), ion channel-related pathways, cell adhesion pathways and pathways related to apoptosis and cell division regulation (Figure 3A). Motif analysis of chromatin regions with differential

accessibility indicated possible altered activity of transcription factors, such as ZNF148 and EGR1. Transcription factor footprinting analysis revealed that these transcription factors were more active in the non-recovery group (Figure 3B,C). Genes of pseudobulk DEG, all variable markers of clusters, pseudobulk DAR, and motif analysis are listed in Tables S3–S7.

Fibroblasts and endothelial cells

Similarly, cell types other than cardiomyocytes were also analysed. In fibroblasts, unsupervised clustering identified 15 subclusters, with differences in distribution observed between groups (Figure S3A). A pseudobulk DEG analysis revealed increased expression of extracellular matrix (ECM) proteins such as *COL1A1*, *COL1A4* and *FN*, as well as *SPARC* in the recovery

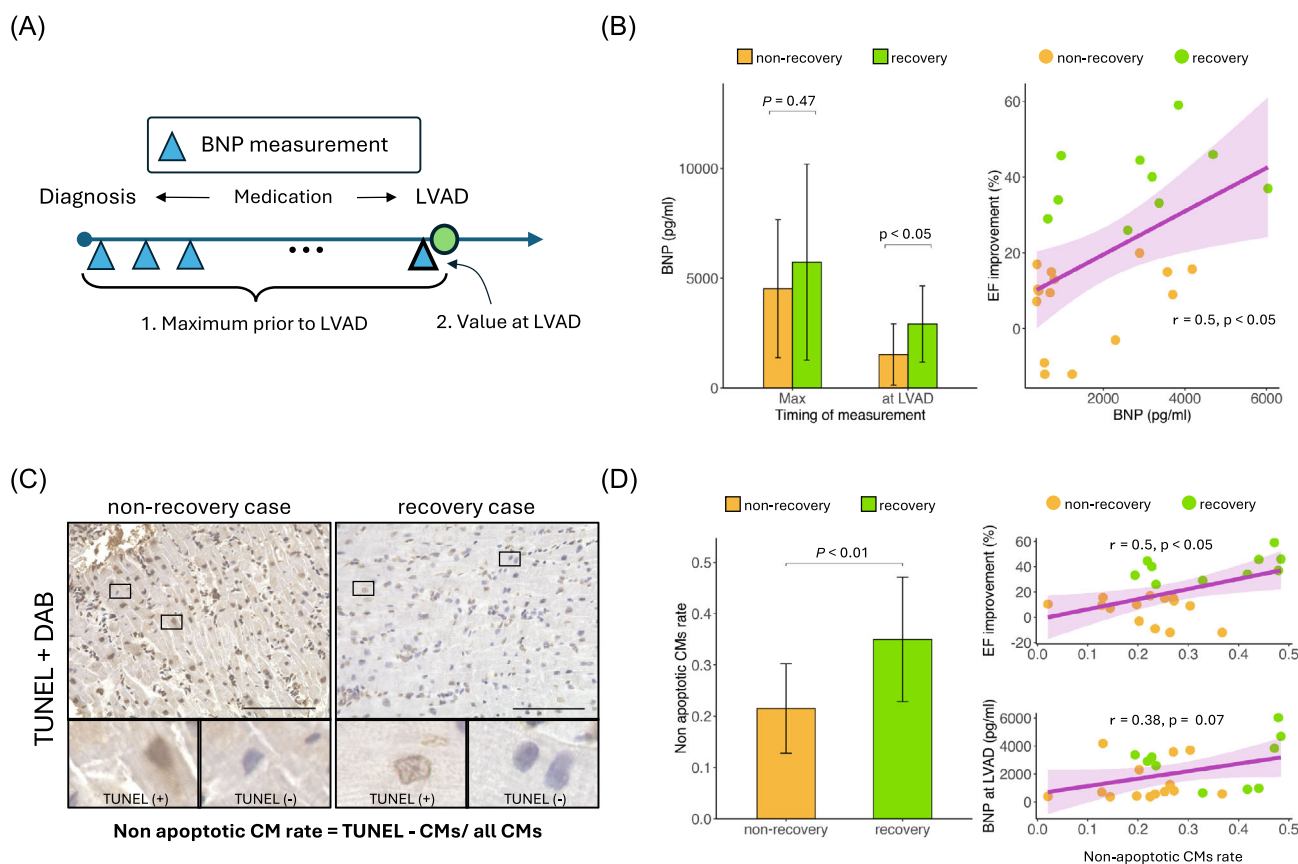
group (Figures S3B,C). Gene ontology-based gene set enrichment analysis further demonstrated significant alterations in pathways related to ECM components, along with alterations in pathways associated with intracellular metabolism (Figure S3D). Endothelial cells were subclustered into 15 groups, and pseudobulk DEG analysis showed findings similar to those of fibroblasts, with increased expression of *COL4A1* and *SPARC*, as well as elevated *IGFBP7* expression in the recovery group (Figures S4A–C). These results are consistent with the observations in fibroblasts, as ECM-related pathways were also enriched in endothelial cells. Additionally, pathways related to interactions with the basement membrane were altered, indicating changes in interactions with surrounding cells in endothelial cells (Figure S4D). To investigate the potential impact on IGF receptor-related pathways involving *IGFBP7*, a cell–cell interaction analysis was performed. However, even in the recovery group, no alterations were observed in the IGF receptor pathway from the endothelium to the cardiomyocytes

(Figure S5). For other cell types, insufficient cell counts and low prediction scores prevented the identification of statistically significant differentially expressed genes.

Histological and serological validation

We focused on validating *NPPB* and its functional products based on RNA/ATAC sequencing results and baseline expression levels. Blood levels of type B natriuretic peptide (BNP), a product of *NPPB*, were measured in all patients prior to LVAD implantation. We analysed BNP values at two time points before LVAD implantation (Figure 4A): the maximum value among all measurements from diagnosis to implantation and the value measured at the time of LVAD implantation. Although there was no significant difference between the outcome in terms of maximum BNP levels during the preoperative period, the BNP levels at LVAD implantation were significantly

Figure 4 Validation of *NPPB* gene and BNP in all cases. (A) Timing of BNP measurements prior to LVAD implantation. The maximum value of all pre-operative measurements and the value immediately before LVAD implantation are enrolled. (B) Left: bar chart of maximum value of prior to LVAD implantation and the value at LVAD implantation. Right: a scatter plot of plasma BNP level at LVAD implantation and EF improvement after LVAD implantation. (C) TdT-mediated dUTP nick end labelling (TUNEL) staining of LV apex samples (×10 magnification). Cells within the rectangle are examples of one of the positive and negative cells. The length of the scale bar is 100 µm. (D) Left: bar chart of TUNEL negative (non-apoptotic) cells proportion. Right-upper: a scatterplot of TUNEL negative cells proportion and EF improvement. Right lower: a scatterplot of TUNEL negative cells proportion and BNP level at LVAD implantation. BNP, type B natriuretic peptide; EF, ejection fraction; LV, left ventricular; LVAD, left ventricular assist device.



higher in the recovery cases [non-recovery: 732 (372–4179) vs. recovery: 3048 (642–6032) pg/mL, $P = 0.04$]. Additionally, BNP levels at LVAD implantation showed a positive correlation with LVEF improvement at 6 months after LVAD implantation ($r = 0.5$, $P = 0.01$) (Figure 4B). As shown in Figure S6, BNP levels were not significantly correlated with age at diagnosis, timing of LVAD implantation or the duration from diagnosis to LVAD implantation ($r = 0.13$, 0.05 , and -0.27 , respectively; all $P > 0.2$). Likewise, TUNEL-positive cell ratios showed no significant association with either age variable ($r = 0.20$ and 0.22 , respectively). In the multivariate logistic regression analysis, including the BNP level at LVAD implantation, age at the diagnosis and the time from the diagnosis to the implantation, while BNP levels at LVAD implantation were not significant independent confounding factors between the recovery and non-recovery groups, they showed a trend towards association with recovery outcomes (Table S7). Figure S7 shows a receiver operating characteristic curve of the BNP level for the LV recovery. The area under the curve was 0.767, and the cut-off value determined by Youden's index was 850 pg/mL.

To further investigate the association between BNP and its anti-apoptotic effects on cardiomyocytes, TUNEL staining of myocardial tissues was performed (Figure 4C). The proportion of TUNEL-negative cardiomyocytes was significantly higher in the recovery cases [vs. non-recovery: 0.21 (0.02–0.37) vs. recovery: 0.37 (0.19–0.48), $P < 0.01$], and the proportion of TUNEL-negative cells showed a positive correlation with the LVEF improvement rate at 6 months after LVAD implantation ($r = 0.5$, $P < 0.05$). While the trend suggested an association between preimplantation BNP levels and the proportion of TUNEL-negative cells, no statistically significant difference was found ($r = 0.38$, $P = 0.06$) (Figure 4D).

To verify the difference in the gene expression of ECM components in fibroblasts, the fibrosis rate of the myocardial tissue was measured. The fibrosis rate did not differ between the two groups [non-recovery: 0.28 (0.06–0.62) % vs. recovery: 0.26 (0.06–0.46) %, $P = 0.5$] and did not significantly correlate with the LVEF improvement rate ($r = -0.03$, $P = 0.89$) (Figure S8). Among the other cells that were not suitable for further analysis, the results of clustering and DEG analysis related to macrophages are shown in Figure S9.

Discussion

This study is the first to use single-nucleus multiomics analysis to elucidate the mechanisms of LV functional recovery following LVAD implantation in paediatric DCM. Twenty-five cases were analysed based on LV functional recovery, with single-nucleus RNA and ATAC sequencing performed on the myocardium at LVAD implantation. The recovery group showed increased *NPPB* expression and chromatin accessibility in cardiomyocytes, with higher serum BNP levels correlat-

ing with LV improvement. TUNEL staining confirmed an association between the anti-apoptotic effects of BNP and recovery.

Miera et al. reported higher recovery rates in patients aged <2 years and those diagnosed with myocarditis.¹⁹ However, their cohort included a substantial proportion of patients with myocarditis and congenital heart disease, and only 57% of patients had a diagnosis of DCM. Conversely, our study focused exclusively on patients with confirmed idiopathic or familial DCM, excluding those with myocarditis based on clinical and histopathological findings. A re-analysis of the DCM-only subgroup in Miera et al.'s data did not show a significant association between younger age and recovery, suggesting that age may not be a universal predictor in DCM cohorts. In our cohort, no significant differences were observed in preoperative or postoperative treatments between groups. Some patients in both groups could not start or titrate beta-blockers or ACEIs preoperatively due to hypotension or shock, but adequate dosing was achieved postoperatively. These results indicate that factors beyond conventional clinical parameters may explain LV functional recovery after LVAD implantation.

Mechanism of altered *NPPB* expression

NPPB is located on chromosome 1, adjacent to *NPPA*, which encodes type A natriuretic peptide. Both genes share a common enhancer region that coordinates and regulates their expression.²⁰ BNP is primarily secreted by cardiomyocytes during heart failure and serves as a serum marker for disease severity.²¹ Through NPR-A and NPR-B receptors, BNP elevates cGMP levels, activating the PKG pathway and exerting anti-apoptotic effects.^{22,23} Alterations in *NPPB* gene expression in these cases may be influenced by both genetic and environmental factors.

Unknown genetic factors related to *NPPB* could result in an alteration of its expression, which influences apoptosis resistance. Gene expression is dynamically regulated by complex mechanisms depending on the cell type and disease state; it has recently been reported that mutations in enhancer regions of sarcomere-related genes affect the DCM phenotype.²⁴ Thus, there is a possibility that patients with DCM also have similar *cis*-regulatory element mutations in *NPPB*. DCM genotypes have been mainly discussed in terms of structural gene mutations, but it may be possible to propose novel genotypes of regulatory mutations in paediatric DCM. *ZNF148* and *EGR1*, which showed increased footprints in the non-recovery group, are reported to be involved in cell growth inhibition and apoptosis promotion, respectively.^{25,26} To detect such regulatory mutations, whole-genome analysis focusing on transcription factors identified in the current ATAC-sequencing study rather than those in whole-exome sequencing will be crucial.

We also should consider the possibility that the preoperative treatment, an environmental factor, influenced *NPPB*

expression levels. Excessive mechanical stress on myocardial cells elevates *NPPB* expression levels, but further increases in load can induce apoptosis.^{27,28} The present results may represent the heterogeneity of preoperative treatment and patient responses. Thus, it is crucial to perform LVAD implantation before apoptosis in cardiomyocytes; *NPPB* gene expression and BNP levels can be clinical markers and therapeutic targets to achieve the bridge-to-recovery approach. A cohort study showed that a population with LV diastolic dysfunction had relatively low blood BNP levels and was more prone to pathologic hypertrophy,²⁹ showing that the existence of subpopulations indicates that BNP is valid as a marker of favourable prognosis. Angiotensin receptor-neprilysin inhibitors (ARNIs), which block the enzyme responsible for degrading natriuretic peptides, have been demonstrated to be superior to conventional heart failure therapies, such as ACEIs.³⁰ ARNIs elevate plasma BNP levels,³¹ making this treatment a strategy aimed at maximizing the cardioprotective effects of BNP itself. A similar role of BNP may be expected for the bridge-to-recovery approach, if further validation with much more cases is performed.

Need for experimental validation of BNP, apoptosis and cell function and applicability to other candidate genes

To confirm those hypotheses, it is necessary to validate the molecular biology of interactions among *NPPB*/BNP, myocardial apoptosis and clinical outcomes. Key challenges include elucidating the quantitative relationships between increased LV volume load in DCM and *NPPB* expression/apoptosis, as well as examining the quantitative effects of BNP supplementation on apoptosis under volume overload conditions. However, robust validation of these relationships is challenging with retrospective study designs. In this context, experimental verification using in vitro or in vivo models and evaluation systems would be particularly valuable. Emerging tools, such as engineered heart tissue models derived from patient-specific iPS cells for cardiomyopathy^{32–34} or DCM model mice developed via genetic modification³⁵ will offer promising platforms for such investigations.

In addition to *NPPB*, other genes such as *MYL7* and *PCDH* family members have shown expression changes. *MYL7* encodes a sarcomere-associated protein involved in cardiomyocyte differentiation and maturation,³⁶ and its expression suggests that cells with differentiation potential may exhibit greater recovery capacity in paediatric DCM. Meanwhile, *PCDH9*, a member of the protocadherin family primarily localized in neuronal membranes, has been linked to cognitive disorders,³⁷ but its function in cardiomyocytes remains unclear. These novel candidate genes, beyond *NPPB*, may also play roles in bridge-to-recovery outcomes. However, downstream protein quantification and functional analyses for

such genes are also difficult within this retrospective study. As gene-editing technology can be used to control the expression of specific genes, disease model-based experimental systems are equally essential for their investigation.³³

Other surrounding cells

In DCM, mechanical stimulation of cardiomyocytes activates fibroblasts, leading to interstitial fibrosis without a reduction in cell numbers. The extent of this fibrosis correlates with cardiac function,³⁸ and previous reports have associated LV functional recovery after LVAD implantation with fibrosis.^{4,5} While fibroblasts exhibited increased expression of ECM components such as collagen and fibronectin, histological analysis revealed no significant differences in the degree of fibrosis. This may suggest either that the progression from elevated gene expression to observable tissue changes requires time, or that gene expression levels reflect fibroblast activation or survival. It is quite possible that there is a gap between the variation in expression of ECM-related genes and the degree of histological fibrosis at a given time point. Moreover, Tsuru et al. isolated cardiac fibroblasts from both paediatric DCM and healthy myocardium and performed in vitro coculture with cardiomyocytes, which demonstrated that fibroblasts derived from DCM exacerbated cardiomyocyte function. They also observed various changes in gene expression, beyond ECM components, between fibroblasts from these two sources. This suggests that, in addition to the quantity of ECM (degree of fibrosis), direct interactions between fibroblasts and cardiomyocytes may influence the DCM phenotype.³⁹ Further investigations are needed to explore the physiological effects of fibroblasts on cardiomyocytes, focusing on the genes that showed alterations in this study. Additionally, IGFBP7, a protein implicated in the development of heart failure,⁴⁰ showed increased expression in vascular endothelial cells. However, no activation of the IGF-1 receptor was observed in cardiomyocytes as the cell–cell interaction analysis showed. This raises the possibility of receptor signalling-inhibition mechanisms, indicating the need for further investigation into intercellular interactions.

Limitations

This was a retrospective, single-centre study with an analysis based on a small sample size. However, this is a multiomics analysis conducted using robust methods on myocardial tissue from a rare disease, which allowed us to identify important candidate genes and propose various molecular mechanisms related to LV functional recovery after LVAD implantation. Based on these results, experimental functional validation using robust methods and prospective clinical studies is

expected to bring us closer to the clinical application of the bridge to recovery.

Conclusions

Single-nucleus multiomics analysis of LV myocardium revealed that increased expression of *NPPB* in cardiomyocytes is associated with LV functional recovery following LVAD implantation in paediatric DCM. The findings suggest milestones and targets to investigate anti-apoptotic effects of BNP for bridge-to-recovery LVAD strategy.

Acknowledgements

We thank the Osaka University COMIT Omics Center for providing the necessary equipment and facilities for sample preparation. We also extend our thanks to the Osaka University Institute of Microbiology for their assistance with library preparation and sequencing for single-cell analysis. Finally, we would like to acknowledge Editage for meticulous English proofreading of this manuscript. Single-nucleus RNA sequencing data are publicly available (Accession number: GSE285315). All single-nucleus ATAC sequence data and corresponding code will be available upon any request.

Funding

This work was supported by JSPS KAKENHI (grant numbers JP20H00542 and JP22K08919).

References

- Singh TP, Cherikh WS, Hsieh E, Chambers DC, Harhay MO, Hayes D, et al. The International Thoracic Organ Transplant Registry of the International Society for Heart and Lung Transplantation: twenty-fourth pediatric heart transplantation report—2021; focus on recipient characteristics. *J Heart Lung Transplant* 2021;**40**:1050-1059. doi:10.1016/j.healun.2021.07.022
- Kanaya T, Ueno T, Taira M, Kido T, Okuda N, Araki K, et al. Impact of long-term support with Berlin Heart EXCOR® in pediatric patients with severe heart failure. *Pediatr Cardiol* 2019;**40**:1126-1133. doi:10.1007/s00246-019-02108-0
- Rohde S, de By TMMH, Bogers AJJC, Schweiger M. Myocardial recovery in children supported with a durable ventricular assist device—a systematic review. *Eur J Cardiothorac Surg* 2023;**64**:ezad263. doi:10.1093/ejcts/ezad263
- Saito S, Matsumiya G, Sakaguchi T, Miyagawa S, Yamauchi T, Kuratani T, et al. Cardiac fibrosis and cellular hypertrophy decrease the degree of reverse remodeling and improvement in cardiac function during left ventricular assist. *J Heart Lung Transplant* 2010;**29**:672-679. doi:10.1016/j.healun.2010.01.007
- Tominaga Y, Ueno T, Kido T, Kanaya T, Narita J, Ishida H, et al. Bridge to recovery with Berlin Heart EXCOR in children <10 kg with dilated cardiomyopathy: a histological analysis. *Eur J Cardiothorac Surg* 2020;**58**:253-260. doi:10.1093/ejcts/ezaa033
- Tominaga Y, Taira M, Watanabe T, Kugo Y, Hasegawa M, Narita J, et al. Cardiomyocyte deoxyribonucleic acid damage and cardiac recovery in paediatric dilated cardiomyopathy. *Eur J Cardiothorac Surg* 2023;**63**:ezad064. doi:10.1093/ejcts/ezad064
- McKenna WJ, Judge DP. Epidemiology of the inherited cardiomyopathies. *Nat Rev Cardiol* 2021;**18**:22-36. doi:10.1038/s41569-020-0428-2
- Pinto YM, Elliott PM, Arbustini E, Adler Y, Anastakis A, Böhm M, et al. Proposal for a revised definition of dilated cardiomyopathy, hypokinetic non-dilated cardiomyopathy, and its implications for clinical practice: A position statement of the ESC working group on myocardial and pericardial diseases. *Eur Heart J* 2016;**37**:1850-1858. doi:10.1093/eurheartj/ehv727

Conflict of interest statement

None declared.

Supporting information

Additional supporting information may be found online in the Supporting Information section at the end of the article.

Data S1. Supporting Information.

Figure S1. Quality control and dimensionality reductions of single nuclei RNA seq.

Figure S2. Preprocessing metrics of single nuclei ATAC seq.

Figure S3. Results of snRNA-seq in Fibroblasts.

Figure S4. Results of snRNA-seq in Endothelium.

Figure S5. Hierarchy plot showing inferred intercellular network through IGF signalling pathway.

Figure S6. Correlation of BNP/TUNEL staining with age- and time-related perioperative factors.

Figure S7. ROC curve of BNP level at LVAD implantation for LV recovery.

Figure S8. Histological validation of left ventricle fibrosis.

Figure S9. UMAP and Volcano plot of Macrophages.

Data S2. Supporting Information.

Table S1. Supporting Information.

Table S2. Supporting Information.

Table S3. Supporting Information.

Table S4. Supporting Information.

Table S5. Supporting Information.

Table S6. Supporting Information.

Table S7. Supporting Information.

9. Arbelo E, Protonotarios A, Gimeno JR, Arbustini E, Barriales-Villa R, Basso C, et al. 2023 ESC guidelines for the management of cardiomyopathies. *Eur Heart J* 2023;44:3503-3626. doi:10.1093/eurheartj/ehad194
10. Zafeiridis A, Jeevanandam V, Houser SR, Margulies KB. Regression of cellular hypertrophy after left ventricular assist device support. *Circulation* 1998;98:656-662. doi:10.1161/01.cir.98.7.656
11. Prescimone T, Masotti S, D'Amico A, Caruso R, Cabiati M, Caselli C, et al. Cardiac molecular markers of programmed cell death are activated in end-stage heart failure patients supported by left ventricular assist device. *Cardiovasc Pathol* 2014;23:272-282. doi:10.1016/j.carpath.2014.04.003
12. Turner AW, Hu SS, Mosquera JV, Ma WF, Hodonsky CJ, Wong D, et al. Single-nucleus chromatin accessibility profiling highlights regulatory mechanisms of coronary artery disease risk. *Nat Genet* 2022;54:804-816. doi:10.1038/s41588-022-01069-0
13. Petti AA, Williams SR, Miller CA, Fiddes IT, Srivatsan SN, Chen DY, et al. A general approach for detecting expressed mutations in AML cells using single cell RNA-sequencing. *Nat Commun* 2019;10:3660. doi:10.1038/s41467-019-11591-1
14. Hetzer R, Kaufmann F, Walter EMD. Paediatric mechanical circulatory support with Berlin Heart EXCOR: development and outcome of a 23-year experience. *Eur J Cardiothorac Surg* 2016;50:203-210. doi:10.1093/ejcts/ezw011
15. Honkoop H, de Bakker DE, Aharonov A, Kruse F, Shakked A, Nguyen PD, et al. Single-cell analysis uncovers that metabolic reprogramming by ErbB2 signaling is essential for cardiomyocyte proliferation in the regenerating heart. *Elife* 2019;8:e50163. doi:10.7554/elife.50163
16. Kallikourdis M, Martini E, Carullo P, Sardi C, Roselli G, Greco CM, et al. T cell costimulation blockade blunts pressure overload-induced heart failure. *Nat Commun* 2017;8:14680. doi:10.1038/ncomms14680
17. Koenig AL, Shchukina I, Amrute J, Andhey PS, Zaitsev K, Lai L, et al. Single-cell transcriptomics reveals cell-type-specific diversification in human heart failure. *Nat Cardiovasc Res* 2022;1:263-280. doi:10.1038/s44161-022-00028-6
18. Kampmann C, Wiethoff CM, Wenzel A, Stolz G, Betancor M, Wippermann CF, et al. Normal values of M mode echocardiographic measurements of more than 2000 healthy infants and children in central Europe. *Heart* 2000;83:667-672. doi:10.1136/heart.83.6.667
19. Miera O, Germann M, Cho MY, Photiadis J, Walter EMD, Hetzer R, et al. Bridge to recovery in children on ventricular assist devices—protocol, predictors of recovery, and long-term follow-up. *J Heart Lung Transplant* 2018;37:1459-1466. doi:10.1016/j.healun.2018.08.005
20. Sergeeva IA, Hooijkaas IB, Ruijter JM, van der Made I, de Groot NE, van der Werken HJ, et al. Identification of a regulatory domain controlling the *Nppa-Nppb* gene cluster during heart development and stress. *Development* 2016;143:2135-2146. doi:10.1242/dev.132019
21. Mukoyama M, Nakao K, Hosoda K, Suga S, Saito Y, Ogawa Y, et al. Brain natriuretic peptide as a novel cardiac hormone in humans. Evidence for an exquisite dual natriuretic peptide system, atrial natriuretic peptide and brain natriuretic peptide. *J Clin Invest* 1991;87:1402-1412. doi:10.1172/jci115146
22. Bon-Mathier AC, Déglise T, Rignault-Clerc S, Biellmann C, Mazzolai L, Rosenblatt-Velin N. Brain natriuretic peptide protects cardiomyocytes from apoptosis and simulates their cell cycle re-entry in mouse infarcted hearts. *Cells* 2022;12:7. doi:10.3390/cells12010007
23. Kuhn M, Holtwick R, Baba HA, Perriard JC, Schmitz W, Ehler E. Progressive cardiac hypertrophy and dysfunction in atrial natriuretic peptide receptor (GC-A) deficient mice. *Heart* 2002;87:368-374. doi:10.1136/heart.87.4.368
24. Gacita AM, Fullenkamp DE, Ohiri J, Pottinger T, Puckelwartz MJ, Nobrega MA, et al. Genetic variation in enhancers modifies cardiomyopathy gene expression and progression. *Circulation* 2021;143:1302-1316. doi:10.1161/circulationaha.120.050432
25. Law DJ, Labut EM, Merchant JL. Intestinal overexpression of ZNF148 suppresses ApcMin/+ neoplasia. *Mamm Genome* 2006;17:999-1004. doi:10.1007/s00335-006-0052-4
26. Boone DN, Qi Y, Li Z, Hann SR. Egr1 mediates p53-independent c-Myc-induced apoptosis via a noncanonical ARF-dependent transcriptional mechanism. *Proc Natl Acad Sci U S A* 2011;108:632-637. doi:10.1073/pnas.1008848108
27. Cheng W, Li B, Kajstura J, Li P, Wolin MS, Sonnenblick EH, et al. Stretch-induced programmed myocyte cell death. *J Clin Invest* 1995;96:2247-2259. doi:10.1172/jci118280
28. Leri A, Claudio PP, Li Q, Wang X, Reiss K, Wang S, et al. Stretch-mediated release of angiotensin II induces myocyte apoptosis by activating p53 that enhances the local renin-angiotensin system and decreases the Bcl-2-to-Bax protein ratio in the cell. *J Clin Invest* 1998;101:1326-1342. doi:10.1172/jci316
29. Okamoto C, Tsukamoto O, Hasegawa T, Matsuo K, Amaki M, Kanzaki H, et al. Relative B-type natriuretic peptide deficiency may exist in diastolic dysfunction in subclinical population. *Circ Rep* 2024;6:151-160. doi:10.1253/circrep.cr-24-0026
30. She J, Lou B, Liu H, Zhou B, Jiang GT, Luo Y, et al. ARNI versus ACEI/ARB in reducing cardiovascular outcomes after myocardial infarction. *ESC Heart Fail* 2021;8:4607-4616. doi:10.1002/ehf2.13644
31. Myhre PL, Vaduganathan M, Claggett B, Packer M, Desai AS, Rouleau JL, et al. B-type natriuretic peptide during treatment with sacubitril/valsartan: the PARADIGM-HF trial. *J Am Coll Cardiol* 2019;73:3073. doi:10.1016/s0735-1097(19)33679-4
32. Miki K, Deguchi K, Nakanishi-Koakutsu M, Lucena-Cacace A, Kondo S, Fujiwara Y, et al. ERRγ enhances cardiac maturation with T-tubule formation in human iPSC-derived cardiomyocytes. *Nat Commun* 2021;12:3596. doi:10.1038/s41467-021-23816-3
33. Hasegawa M, Miki K, Kawamura T, Sasozaki IT, Higashiyama Y, Tsuchida M, et al. Gene correction and overexpression of TNNI3 improve impaired relaxation in engineered heart tissue model of pediatric restrictive cardiomyopathy. *Dev Growth Differ* 2024;66:119-132. doi:10.1111/dgd.12909
34. Wang BZ, Nash TR, Zhang X, Rao J, Abriola L, Kim Y, et al. Engineered cardiac tissue model of restrictive cardiomyopathy for drug discovery. *Cell Rep Med* 2023;4:100976. doi:10.1016/j.xcrm.2023.100976
35. Yun HH, Jung SY, Park BW, Ko JS, Yoo K, Yeo J, et al. An adult mouse model of dilated cardiomyopathy caused by inducible cardiac-specific *Bis* deletion. *Int J Mol Sci* 2021;22:1343. doi:10.3390/ijms22031343
36. Latinkić BV, Cooper B, Smith S, Kotecha S, Towers N, Sparrow D, et al. Transcriptional regulation of the cardiac-specific *MLC2* gene during *Xenopus* embryonic development. *Development* 2004;131:669-679. doi:10.1242/dev.00953
37. Xiao X, Zheng F, Chang H, Ma Y, Yao YG, Luo XJ, et al. The gene encoding protocadherin 9 (PCDH9), a novel risk factor for major depressive disorder. *Neuropsychopharmacology* 2018;43:1128-1137. doi:10.1038/npp.2017.243
38. Assomull RG, Prasad SK, Lyne J, Smith G, Burman ED, Khan M, et al. Cardiovascular magnetic resonance, fibrosis, and prognosis in dilated cardiomyopathy. *J Am Coll Cardiol* 2006;48:1977-1985. doi:10.1016/j.jacc.2006.07.049
39. Tsuru H, Yoshihara C, Sugino H, Matsumoto M, Ishii Y, Narita J, et al. Pathogenic roles of cardiac fibroblasts in pediatric dilated cardiomyopathy. *J Am Heart Assoc* 2023;12:e029676. doi:10.1161/jaha.123.029676
40. Zhang L, Smyth D, Al-Khalaf M, Blet A, Du Q, Bernick J, et al. Insulin-like growth factor-binding protein-7 (IGFBP7) links senescence to heart failure. *Nat Cardiovasc Res* 2022;1:1195-1214. doi:10.1038/s44161-022-00181-y